

Are your **MRI contrast agents** cost-effective?

Learn more about generic **Gadolinium-Based Contrast Agents**.



**FRESENIUS  
KABI**

caring for life

# AJNR

## **Dynamic Contrast–Enhanced MRI Parameters and Normalized ADC Values Could Aid Differentiation of Skull Base Osteomyelitis from Nasopharyngeal Cancer**

A. Baba, R. Kurokawa, M. Kurokawa, Y. Ota and A.  
Srinivasan

This information is current as  
of April 18, 2024.

*AJNR Am J Neuroradiol* published online 15 December  
2022

<http://www.ajnr.org/content/early/2022/12/15/ajnr.A7740>

# Dynamic Contrast-Enhanced MRI Parameters and Normalized ADC Values Could Aid Differentiation of Skull Base Osteomyelitis from Nasopharyngeal Cancer

 A. Baba,  R. Kurokawa,  M. Kurokawa,  Y. Ota, and  A. Srinivasan



## ABSTRACT

**BACKGROUND AND PURPOSE:** The skull base osteomyelitis sometimes can be difficult to distinguish from nasopharyngeal cancer. This study aimed to investigate the differences between skull base osteomyelitis and nasopharyngeal cancer using dynamic contrast-enhanced MR imaging and normalized ADC values.

**MATERIALS AND METHODS:** This study included 8 and 12 patients with skull base osteomyelitis and nasopharyngeal cancer, respectively, who underwent dynamic contrast-enhanced MR imaging and DWI before primary treatment. Quantitative dynamic contrast-enhanced MR imaging parameters and ADC values of the ROIs were analyzed. Normalized ADC parameters were calculated by dividing the ROIs of the lesion by that of the spinal cord.

**RESULTS:** The rate transfer constant between extravascular extracellular space and blood plasma per minute (Kep) was significantly lower in patients with skull base osteomyelitis than in those with nasopharyngeal cancer (median, 0.43 versus 0.57;  $P = .04$ ). The optimal cutoff value of Kep was 0.48 (area under the curve, 0.78; 95% CI, 0.55–1). The normalized mean ADC was significantly higher in patients with skull base osteomyelitis than in those with nasopharyngeal cancer (median, 1.90 versus 0.87;  $P < .001$ ). The cutoff value of normalized mean ADC was 1.55 (area under the curve, 0.96; 95% CI, 0.87–1). The area under the curve of the combination of dynamic contrast-enhanced MR imaging parameters (Kep and extravascular extracellular space volume per unit tissue volume) was 0.89 (95% CI, 0.73–1), and the area under the curve of the combination of dynamic contrast-enhanced MR imaging parameters and normalized mean ADC value was 0.98 (95% CI, 0.93–1).

**CONCLUSIONS:** Quantitative dynamic contrast-enhanced MR imaging parameters and normalized ADC values may be useful in differentiating skull base osteomyelitis and nasopharyngeal cancer. The combination of dynamic contrast-enhanced MR imaging parameters and normalized ADC values outperformed each measure in isolation.

**ABBREVIATIONS:** AUC = area under the curve; DCE = dynamic contrast-enhanced; EES = extravascular extracellular space;  $K^{trans}$  = volume transfer constant between extravascular extracellular space and blood plasma per minute; Kep = rate transfer constant between EES and blood plasma per minute;  $nADC_{mean}$  = normalized mean ADC; NPC = nasopharyngeal cancer; Ve = EES volume per unit tissue volume; Vp = plasma volume; SBO = skull base osteomyelitis

Skull base osteomyelitis (SBO) is a rare and potentially life-threatening infection of the skull base.<sup>1</sup> SBO is typically caused by an inadequately treated ear or paranasal infection in patients with diabetes, older age, or immune suppression.<sup>1–3</sup> Mucosal pathology and biopsy culture are important approaches for the diagnosis of SBO, and diagnostic imaging has a complementary value when necessary to exclude the malignant potential.<sup>1,4,5</sup> However,


SBO sometimes can be difficult to distinguish from malignancies clinically and radiologically, especially nasopharyngeal cancer (NPC). Radiologically, SBO may show masslike, asymmetric soft-tissue involvement, and NPC may show skull base involvement, making the diagnosis challenging. To date, there have been no reliable studies to differentiate SBO and NPC on MR imaging morphologic findings, and no imaging characteristics have been established to clearly distinguish these 2 diseases.<sup>6</sup> There is only a report of the utility of ADC values in DWI in quantitatively differentiating SBO from malignancy,<sup>7</sup> and the clinical utility and significance of this diagnostic method are noteworthy.

Dynamic contrast-enhanced MR imaging (DCE-MR imaging) is a contrast-enhanced perfusion imaging technique, and several quantitative parameters can be obtained on the basis of this technique. DCE-MR imaging has been used to differentiate neoplastic and non-neoplastic lesions,<sup>8,9</sup> though the evidence for DCE-MR

Received August 11, 2022; accepted after revision November 15.

From the Division of Neuroradiology (A.B., R.K., M.K., Y.O., A.S.), Department of Radiology, University of Michigan, Ann Arbor, Michigan; and Department of Radiology (A.B.), The Jikei University School of Medicine, Tokyo, Japan.

Please address correspondence to Akira Baba, MD, PhD, Division of Neuroradiology, Department of Radiology, University of Michigan, 1500 E. Medical Center Dr, Ann Arbor, MI 48109; e-mail: akirababa0120@gmail.com

 Indicates article with online supplemental data.

<http://dx.doi.org/10.3174/ajnr.A7740>

imaging in differentiating SBO from NPC has not been reported. This study aimed to evaluate the diagnostic performance for differentiating SBO and NPC using ADC and DCE-MR imaging parameters.

## MATERIALS AND METHODS

We obtained our institutional review board exemption for this retrospective study from University of Michigan, and patient consent was waived. Data were acquired in compliance with all applicable Health Insurance Portability and Accountability Act regulations. All procedures followed were in accordance with the Helsinki Declaration of 1975, as revised in 2008. Data were de-identified before any analysis.

### Patients

Consecutive patients diagnosed with SBO and NPC who underwent both pretreatment DCE-MR imaging and pretreatment DWI between December 2015 and February 2022 were included. All included patients were imaged using Ingenia and Achieva systems (Philips Healthcare). Patients were considered to have SBO if they had a clinical history suggestive of osteomyelitis, with pathologically proved inflammatory changes or culture-proved causative bacteria and improvement with subsequent treatment. As for SBO, we excluded 8 patients who had been previously treated with surgery or radiation therapy for tumors proximal to the skull base so that we could avoid encountering any overlap in imaging features between SBO and posttreatment changes in the same patient that would make the analysis difficult. All NPC cases were pathologically confirmed.

### MR Imaging Acquisition

MR imaging examinations were performed using 1.5T ( $n = 10$ ) and 3T ( $n = 10$ ) MR imaging systems (Ingenia, Achieva; Philips Healthcare). DWI was performed with b-values of 0 and 1000  $s/mm^2$  and the following parameters: TR range, 3500–11,000 ms; TE range, 70–92 ms; number of excitations, 1–2; section thickness/gap, 4–6/0–1 mm; FOV, 225–255  $\times$  235–255 mm; matrix, 140–200  $\times$  130–200; and 3 diffusion directions. DCE-MR imaging was performed via 3D T1-weighted fast-field echo. Parameters for 3D T1-weighted fast-field echo were as follows: TR, 4.4–4.8 ms; TE, 2 ms; flip angles, 30°; section thickness/gap, 5/–2.5 mm; FOV, 240  $\times$  240 mm; matrix, 240  $\times$  240; number of excitations, 1; number of slices per dynamic scan, 48; temporal resolution, 8.8 seconds; total acquisition time, 4 minutes 24 seconds. An intravenous bolus of 20 mL of gadobenate dimeglumine contrast (MultiHance; Bracco Diagnostics) was administered through a peripheral arm vein using a power injector with a flow rate of 5.0 mL/s, followed by a 20-mL saline flush.

### Data Analysis

The demographic characteristics, including age, sex, the presence of ear or paranasal sinus lesions, a history of diabetes mellitus, cranial nerve symptoms, pathology, causative culture bacteria, treatment method, and clinical course, of patients with SBO and the characteristics, including age, sex, pathology, and T classification, of patients with NPC were reviewed from the electronic medical records.

### ADC Analysis

ADC maps were constructed by a monoexponential fitting model using OleaSphere (Version 3.0; Olea Medical). Two board-certified radiologists with 9 and 13 years of experience outlined 3 separate ROIs on the ADC maps, predominantly including the low-signal region while excluding cystic or necrotic regions from ROIs with consensus. Another ROI for ADC was placed as a reference in the spinal cord,<sup>10</sup> which was seen in the same section imaging. ROI sizes ranged from 7 to 18 mm.<sup>2</sup> For each ROI, the normalized mean ADC ( $nADC_{mean}$ ) was calculated by dividing the mean ADC by the reference mean ADC of the spinal cord. The  $nADC_{mean}$  of 3 ROIs was averaged.

### DCE Analysis

Quantitative DCE-MR imaging analysis was performed using OleaSphere (Version 3.0) on the basis of the extended Tofts model, by which pixel-based parameter maps are calculated from time-intensity curves. An arterial input function was calculated automatically using cluster analysis techniques, and deconvolution of the arterial input function was performed with a time-insensitive block-circulant singular-value decomposition.<sup>11</sup> The 2 board-certified radiologists with 9 and 13 years of experience outlined 3 separate ROIs in the lesions on permeability maps, predominantly including the enhancing components while excluding cystic or necrotic regions from the ROIs with consensus. The calculated quantitative vascular permeability parameters were as follows; extravascular extracellular space (EES), volume per unit tissue volume ( $V_e$ ), fractional plasma volume ( $V_p$ ), volume transfer constant between EES and blood plasma per minute ( $K^{trans}$ ), and rate transfer constant between EES and blood plasma per minute ( $K_{ep}$ ).

### Statistical Analyses

Shapiro-Wilk tests were performed to confirm the normality of distribution in each numeric parameter. The Mann-Whitney U test was used to compare DCE-MR imaging quantitative parameters ( $V_p$ ,  $V_e$ ,  $K^{trans}$ ,  $K_{ep}$ ) and  $nADC_{mean}$  between SBO and NPC. Two-sided  $P$  values  $< .05$  were considered statistically significant. For parameters with 2-sided  $P$  values  $< .20$ , the optimal cutoff values in the receiver operating characteristics analysis were determined as values to maximize the Youden index (sensitivity + specificity – 1).<sup>12</sup> Diagnostic performances were calculated on the basis of the cutoff values. The area under the receiver operating characteristic curve of the combination parameters was calculated. All statistical analyses were performed using R statistical and computing software, Version 3.6.1 (<http://www.r-project.org/>).

## RESULTS

### Patients

In this study, 20 patients were included, 8 and 12 of whom had SBO and NPC, respectively. Patients' demographic and clinical data are summarized in Online Supplemental Data and Table 1.

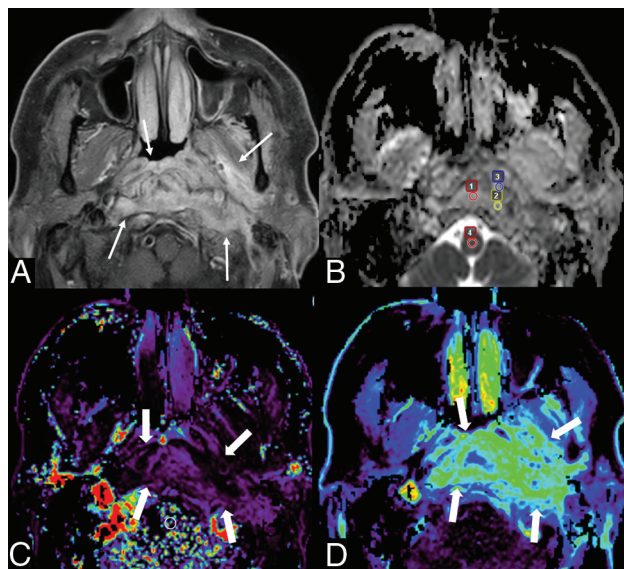
Half of the patients with SBO had ear lesions, followed by sinus lesions. All patients with SBO had diabetes mellitus. Many patients with SBO presented with cranial nerve symptoms, with cranial nerve XII symptoms being the most common. Cultured causative bacteria of SBO were *Pseudomonas aeruginosa*, *Staphylococcus aureus*, and culture-negative.

**Table 1: Demographic and clinical information of nasopharyngeal cancer**

Clinical Information	
Demographic	
Sex	Male = 8, female = 4
Median age (range) (yr)	52.5 (36–69)
Clinical	
Pathology	
Squamous cell carcinoma	12/12 (100.0%)
T classification	
T1	2/12 (16.7%)
T2	5/12 (41.7%)
T3	2/12 (16.7%)
T4	3/12 (25.0%)

**Table 2: DCE-MR imaging and ADC parameters<sup>a</sup>**

DCE Parameters	SBO	Nasopharyngeal Cancer	P Value
Ve	0.48 (0.36–0.55)	0.38 (0.14–0.63)	.15
Vp	0.14 (0.04–2.36)	0.12 (0.05–0.26)	.99
$K^{trans}$ ( $\text{min}^{-1}$ )	0.20 (0.15–0.39)	0.28 (0.06–1.42)	.51
Kep ( $\text{min}^{-1}$ )	0.43 (0.31–0.48)	0.57 (0.31–3.70)	.04 <sup>b</sup>
ADC value	1.48 (1.14–1.84)	0.69 (0.55–1.39)	<.001 <sup>b</sup>
Reference ADC	0.79 (0.54–0.94)	0.81 (0.73–0.90)	.39
nADC <sub>mean</sub>	1.90 (0.61–2.48)	0.87 (0.61–1.90)	<.001 <sup>b</sup>

<sup>a</sup>Data are median and range.<sup>b</sup>Statistically significant.**FIG 1.** A case of SBO in a 68-year-old man. Postcontrast fat-suppressed T1-weighted image (A) shows ill-defined enhancement in the nasopharynx, prevertebral space, left parapharyngeal space, and left masticator space (arrows). The ADC map (B) shows 3 ROIs (Nos. 1–3, small circles) within high-signal lesion and 1 ROI (No. 4, small circle) for reference in the spinal cord, with an nADC<sub>mean</sub> of 1.86. DCE-MR imaging (C, Kep map; D, Ve map) shows the lesion (thick arrows) with a Kep of 0.42  $\text{minute}^{-1}$  and Ve of 0.54.

### DCE-MR Imaging and ADC Parameters

The results of DCE-MR imaging and ADC analyses are summarized in Table 2. A pulsed input pattern was observed in the arterial input function curves in all patients. Kep was significantly lower in patients with SBO than in those with NPC ( $P = .04$ ). The optimal

cutoff value of Kep was 0.48 (area under the curve [AUC], 0.78; 95% CI, 0.55–1), and that of Ve was 0.43 (AUC, 0.70; 95% CI, 0.45–0.95). The nADC<sub>mean</sub> was significantly higher in patients with SBO than in those with NPC ( $P < .001$ ). The optimal cutoff value of the nADC<sub>mean</sub> was 1.55 (AUC, 0.96; 95% CI, 0.87–1). Representative MR images of SBO and NPC are demonstrated in Figs 1 and 2. The AUC of the combination of DCE-MR imaging parameters (Kep and Ve) was 0.89 (95% CI, 0.73–1), and the AUC of the combination of DCE-MR imaging parameters and the nADC<sub>mean</sub> was 0.98 (95% CI, 0.93–1). The decision tree in differentiating SBO and NPC is shown in Fig 3.

### DISCUSSION

This study evaluated the characteristics and differences in the quantitative parameters from DCE-MR imaging and normalized ADC values in DWI between SBO and NPC. Kep and nADC<sub>mean</sub> showed significant differences between SBO and NPC. The combined Kep and Ve and the nADC<sub>mean</sub> had a remarkably high AUC of 0.98 for differentiating SBO and NPC.

SBO is typically associated with an improperly treated ear or paranasal sinus infections in older patients with diabetes or those who are immunocompromised.<sup>1–3</sup> Previous studies have reported a high incidence of ear and paranasal sinus complications,<sup>2,13</sup> and in the present study, ear (50%) and paranasal sinus (25%) lesions were identified. Approximately half of the patients had histories of diabetes,<sup>1,2,13</sup> and all patients in the current study had diabetes. Cranial nerve symptoms were observed in 57%–83% of patients<sup>1,2</sup> and were noted in many patients in the present study (75%). *P. aeruginosa* and *S aureus* have been reported as the major causative pathogens,<sup>1,2,13</sup> and the results were similar in the present study.

Mucosal pathology and biopsy culture are important clinical approaches in the diagnosis of SBO. However, when pathology results are false-negative or inconclusive, when cultures are negative, or when disease persists despite appropriate antibiotic therapy, it is clinically important to rule out malignant possibilities, including nasopharyngeal cancer.<sup>1,4,5</sup> Additionally, diagnostic imaging with MR imaging has clinical value in providing complementary assistance for ruling these out.<sup>1,4,5</sup>

SBO is associated with cranial nerve symptoms such as dysphagia and facial paralysis, which can clinically mimic a malignant tumor of the skull base.<sup>6</sup> Therefore, the biopsy and culture described above are essential to differentiate SBO from malignant lesions,<sup>14</sup> and more alarming, there are culture-negative SBO cases.<sup>15–17</sup> These clinical challenges often delay the diagnosis of SBO.<sup>2,18</sup> In addition, radiological imaging plays an important role in establishing a diagnosis, estimating disease extent, and monitoring the treatment response of SBO,<sup>19</sup> which can sometimes clinically mimic malignancy by presenting masslike and asymmetric soft-tissue infiltrates, making the diagnosis difficult.<sup>2,3,6,14,15,20</sup> Therefore, identifying quantitative imaging indicators to diagnose SBO radiologically is important.

DWI is a noninvasive MR imaging sequence used to visualize changes in the motion of water molecules and is a surrogate marker of cell density. The ADC value, a parameter calculated from DWI, has been useful in distinguishing benign from malignant head and neck tumors and in distinguishing recurrence



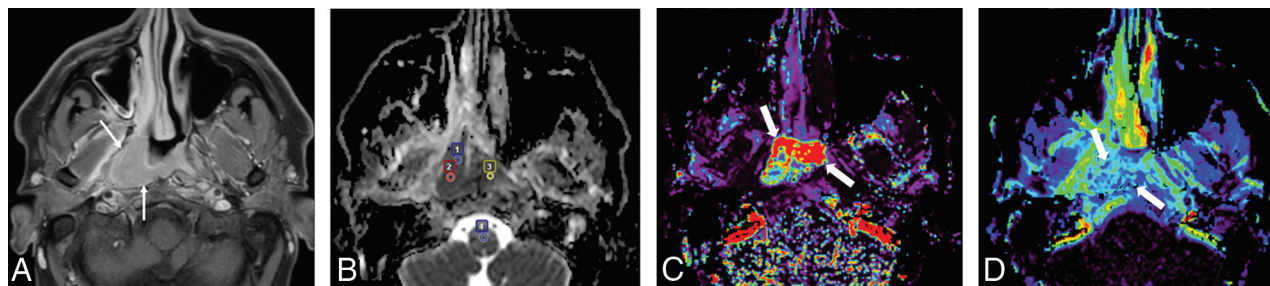


**FIG 2.** A case of nasopharyngeal cancer in a 37-year-old man. A mass lesion with enhancement (arrows) mainly on the right side of the nasopharynx is observed on the postcontrast fat-suppressed T1-weighted image (A). An ADC map (B) shows 3 ROIs (Nos. 1–3, small circles) within a low-signal lesion and 1 ROI (No. 4, small circle) for reference in the spinal cord, with an  $nADC_{\text{mean}}$  of 0.86. DCE-MR imaging (C, Kep map; D, Ve map) shows the lesion (thick arrows) with a Kep of  $3.14 \text{ minute}^{-1}$  and a Ve of 0.36.

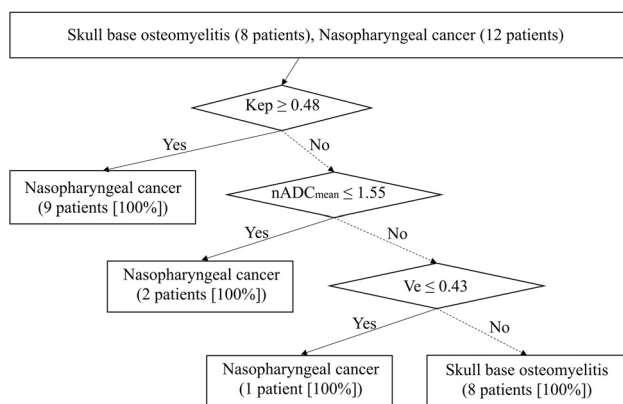


**FIG 3.** The decision tree model incorporating DCE parameters (Kep and Ve) and the  $nADC_{\text{mean}}$ .

from posttreatment changes of head and neck cancers.<sup>21,22</sup> Ozgen et al<sup>7</sup> reported the utility of ADC values in differentiating SBO from skull base malignancies. The study showed that SBO had significantly higher ADC values compared with skull base malignancies (mean ADC value, 1.26 versus 0.75 [NPC], 0.59 [malignant lymphoma], and 0.99 [metastasis]  $\times 10^{-3} \text{ mm}^2$ ) and a cutoff value of  $1.08 \times 10^{-3} \text{ mm}^2$  with a sensitivity of 0.89, specificity of 0.86, and accuracy of 0.86.<sup>7</sup>

Because absolute ADC values can vary from scanner to scanner on the basis of the model and Tesla strength, we attempted to reduce this variability by normalizing the lesion ADC value with an internal standard, in this case the spinal cord ADC. In the present study, SBO showed significantly higher normalized ADC values than NPC, with a sensitivity of 0.92, specificity of 1.00, and AUC of 0.96 when the cutoff value was set at 1.55, indicating high diagnostic performance. As in the previous report, normalized ADC is also useful for diagnosing both. Normalization of ADC is considered valuable for correcting for age and intermodel differences.<sup>12,23</sup> In addition, there has been no study investigating the use of normalized ADC values in DWI in differentiating SBO from NPC.

DCE-MR imaging has been used to differentiate neoplastic and non-neoplastic pathologies using its quantitative and semi-quantitative parameters.<sup>8,9</sup> However, the diagnostic role of DCE-MR imaging in differentiating SBO and malignancies is unknown. In the present study, the combined AUC of Kep and Ve was 0.89.

Furthermore, the combination of DCE-MR imaging parameters and the  $nADC_{\text{mean}}$  showed a remarkably high AUC value of 0.98. DCE-MR imaging parameters and  $nADC_{\text{mean}}$  are quantitative information that can be obtained during a single MR imaging procedure, and the combined evaluation of these parameters and their clinical application might be beneficial to patients.

The present study has some limitations. This was a single-center, retrospective study with a small number of patients. Future studies with a larger number of patients are warranted.

## CONCLUSIONS

The combination of quantitative DCE-MR imaging parameters and normalized ADC values showed high diagnostic performance and may be useful in differentiating SBO and NPC. The combination of DCE-MR imaging parameters and normalized ADC values outperformed each measure in isolation.

Disclosure forms provided by the authors are available with the full text and PDF of this article at [www.ajnr.org](http://www.ajnr.org).

## REFERENCES

1. Johnson AK, Batra PS. Central skull base osteomyelitis: an emerging clinical entity. *Laryngoscope* 2014;124:1083–87 [CrossRef Medline](#)
2. Álvarez Jáñez F, Barriga LQ, Iñigo TR, et al. Diagnosis of skull base osteomyelitis. *Radiographics* 2021;41:156–74 [CrossRef Medline](#)
3. Chang PC, Fischbein NJ, Holliday RA. Central skull base osteomyelitis in patients without otitis externa: imaging findings. *AJNR Am J Neuroradiol* 2003;24:1310–16 [Medline](#)
4. Khan M, Quadri S, Kazmi A, et al. A comprehensive review of skull base osteomyelitis: diagnostic and therapeutic challenges among various presentations. *Asian J Neurosurg* 2018;13:959–70 [CrossRef Medline](#)
5. Auinger AB, Dahm V, Stanisz I, et al. The challenging diagnosis and follow-up of skull base osteomyelitis in clinical practice. *Eur Arch Otorhinolaryngol* 2021;278:4681–88 [CrossRef Medline](#)
6. van Kroonenburgh AM, van der Meer WL, Bothof RJ, et al. Advanced imaging techniques in skull base osteomyelitis due to malignant otitis externa. *Curr Radiol Rep* 2018;6:3 [CrossRef Medline](#)
7. Ozgen B, Oguz KK, Cila A. Diffusion MR imaging features of skull base osteomyelitis compared with skull base malignancy. *AJNR Am J Neuroradiol* 2011;32:179–84 [CrossRef Medline](#)
8. Morabito R, Alafaci C, Pergolizzi S, et al. DCE and DSC perfusion MRI diagnostic accuracy in the follow-up of primary and metastatic intra-axial brain tumors treated by radiosurgery with CyberKnife. *Radiat Oncol* 2019;14:65 [CrossRef Medline](#)
9. Albano D, Bruno F, Agostini A, et al; the Young SIRM Working Group. Dynamic contrast-enhanced (DCE) imaging: state of the art

- and applications in whole-body imaging. *Jpn J Radiol* 2022;40:341–66 [CrossRef Medline](#)
10. Koontz NA, Wiggins RH. **Differentiation of benign and malignant head and neck lesions with diffusion tensor imaging and DWI.** *AJR Am J Roentgenol* 2017;208:1110–15 [CrossRef Medline](#)
  11. Mouridsen K, Christensen S, Gyldensted L, et al. **Automatic selection of arterial input function using cluster analysis.** *Magn Reson Med* 2006;55:524–31 [CrossRef Medline](#)
  12. Kurokawa R, Kurokawa M, Baba A, et al. **Dynamic susceptibility contrast-MRI parameters, ADC values, and the T2-FLAIR mismatch sign are useful to differentiate between H3-mutant and H3-wild-type high-grade midline glioma.** *Eur Radiol* 2022;32:3672–82 [CrossRef Medline](#)
  13. Prasad SC, Prasad KC, Kumar A, et al. **Osteomyelitis of the temporal bone: terminology, diagnosis, and management.** *J Neurol Surg B Skull Base* 2014;75:324–31 [CrossRef Medline](#)
  14. Singhal A, Sotoudeh H, Chapman PR. **Skull base osteomyelitis imaging.** *Curr Opin Otolaryngol Head Neck Surg* 2021;29:333–41 [CrossRef Medline](#)
  15. See A, Tan TY, Gan EC. **Atypical culture-negative skull base osteomyelitis masquerading as advanced nasopharyngeal carcinoma.** *Am J Otolaryngol* 2016;37:236–39 [CrossRef Medline](#)
  16. Sokołowski J, Lachowska M, Karchier E, et al. **Skull base osteomyelitis: factors implicating clinical outcome.** *Acta Neurol Belg* 2019;119:431–37 [CrossRef Medline](#)
  17. Spielmann PM, Yu R, Neeff M. **Skull base osteomyelitis: current microbiology and management.** *J Laryngol Otol* 2013;127(127 Suppl 1):8–12 [CrossRef Medline](#)
  18. Mahdyou P, Pulcini C, Gahide I, et al. **Necrotizing otitis externa: a systematic review.** *Otol Neurotol* 2013;34:620–29 [CrossRef Medline](#)
  19. Vaidyanathan S, Lingam RK. **Imaging of acute and chronic skull base infection.** *Neuroimaging Clin N Am* 2021;31:571–98 [CrossRef Medline](#)
  20. Ganhewa AD, Kuthubutheen J. **A diagnostic dilemma of central skull base osteomyelitis mimicking neoplasia in a diabetic patient.** *BMJ Case Rep* 2013;2013:bcr2012007183 [CrossRef](#)
  21. Surov A, Meyer HJ, Wienke A. **Apparent diffusion coefficient for distinguishing between malignant and benign lesions in the head and neck region: a systematic review and meta-analysis.** *Front Oncol* 2019;9:1362 [CrossRef Medline](#)
  22. Baba A, Kurokawa R, Kurokawa M, et al. **ADC for differentiation between posttreatment changes and recurrence in head and neck cancer: a systematic review and meta-analysis.** *AJNR Am J Neuroradiol* 2022;43:442–47 [CrossRef Medline](#)
  23. Ding X, Xu H, Zhou J, et al. **Reproducibility of normalized apparent diffusion coefficient measurements on 3.0-T diffusion-weighted imaging of normal pancreas in a healthy population.** *Medicine (Baltimore)* 2019;98:e15104 [CrossRef Medline](#)